International Journal of Heat and Mass Transfer 54 (2011) 5149–5162

Contents lists available at SciVerse ScienceDirect

International Journal of Heat and Mass Transfer

journal homepage: www.elsevier.com/locate/ijhmt

Experimental quantification of heat and mass transfer process through vegetated roof samples in a new laboratory setup

Paulo Cesar Tabares-Velasco [1], Jelena Srebric *

Department of Architectural Engineering, The Pennsylvania State University, 222 Engineering Unit A, University Park, PA 16802-1417, United States

ARTICLE INFO

Article history:
Received 15 April 2010
Received in revised form 20 August 2011
Accepted 20 August 2011
Available online 14 September 2011

Keywords:
Green roofs
Planted roofs
Heat and mass transfer
Evapotranspiration
Energy balance

ABSTRACT

A new experimental apparatus, "Cold Plate", was designed and built to quantify heat and mass transfer processes for green roof samples inside an environmental chamber. The "Cold Plate" apparatus addressed shortcomings in the existing data sets available for green roof energy balance calculations. Experimental data collected in this apparatus show that evapotranspiration controlled the intensity of all other heat fluxes, depending on the plant and environmental conditions. Also, under the described laboratory conditions, the uninsulated green roof samples with plants showed an average heat flux reduction of 25% compared to samples without plants. This reduction was due to the plants providing extra shading, additional water storage and better water control mechanisms.

1. Introduction

Green roofs are regarded as a sustainable technology that offers several benefits to the society. These benefits are: reduced energy demand for space conditioning, reduced storm-water runoff, expanded lifetime of roofing membranes as well as reduced urban heat island effect when implemented in entire neighborhoods. In general, green or vegetated roofs are specialized roofing systems that support vegetation growth on rooftops [1,2]. Green roofs typically consist of several layers, which include following materials from the top to the bottom of an assembly: (1) drought tolerant plants such as *Sedum* and *Delosperma* species, (2) substrate or engineered soil, (3) filter or cloth membrane, (4) drainage layer, and (5) root resistant layer [1,3]. The plant and substrate layers reduce direct thermal loads, and, therefore, create energy benefits on a green roof via several transport mechanisms that include transfer of both heat and water.

Energy benefits from green roofs have been previously studied by theoretical, experimental and/or a combination of both approaches. From these approaches, the experimental approach has the benefit of its reliability and simplicity as long as an experimental setup is available. Previous field studies have measured one or several of the following parameters: (1) heat flux reduction through the roof, (2) green roof *R*-values, and (3) evapotranspiration for unsteady weather conditions. Additionally, there have been few laboratory studies focused on quantifying the same transport processes.

Several important field experimental studies of green roofs in North America have compared the thermal performance of green roofs for summer weather conditions. Average heat flux reduction through these roofs varied from 18% to 75% when green roof layers were installed [2,4–10]. A large variation of heat flux reduction could be attributed to experimental setups, plant coverage, building design, and local weather conditions. Interestingly, a field study [7] and our laboratory study [11] have found a significant reduction of heat flux from a green roof compared to a bare soil roof. The laboratory analysis found that it is not just the shading, but also the evapotranspiration that improves the thermal performance of the green roof with the presence of plants [12]. This finding was possible due to tightly controlled laboratory experiments with laboratory graded instrumentation.

Calculated *R*-values for green roofs with a shallow substrate (7.5–15 cm depth) measured in field and laboratories experiments varied from 0.37 to 0.85 m^2K/W (1.8–4.8 ft^2 h °F/Btu) [7,11,13]. The difficulty in measuring and then calculating the *R*-value was due to the non-steady state conditions during the test periods [14,15], while *R*-value is by definition a steady-state property that indicates a thermal resistance of homogenous building materials. Thus, due to inhomogeneous green roof layers as well as dynamic heat and mass transfer processes in green roofs, the thermal resistance cannot be modeled with a simple *R*-value used for conventional building materials.

Previous research has shown that the substrate water content plays an important role in decreasing the surface green roof

* Corresponding author.
E-mail address: jsrebric@engr.psu.edu (J. Srebric).
[1] Present address: National Renewable Energy Laboratory, 1617 Cole Blvd. MS 5202, Golden, CO 80401, United States. Tel.: +1 303 384 7591; fax: +1 303 384 7495.

0017-9310/$ - see front matter © 2011 Elsevier Ltd. All rights reserved.
doi:10.1016/j.ijheatmasstransfer.2011.08.034

Nomenclature

LAI	leaf area index [(leaf area)/(soil surface)]
M	metabolic storage (photosynthesis and respiration) (W/m^2)
$Q_{conduction}$	conductive heat flux through roof (W/m^2)
Q_{ET}	evapotranspiration, or latent heat flux by convection (W/m^2)
Q_{IR}	long-wave radiation (W/m^2)
$Q_{sensible}$	sensible heat flux by convection (W/m^2)
R_n	net radiation (W/m^2)
$S_{thermal}$	thermal storage for substrate, plants (W/m^2)
VWC	substrate volumetric water content
r_s	stomatal resistance to mass transfer (s/m)
γ	psychrometric constant = $C_pP/0.622i_{fg}$
h_{conv}	convective heat transfer coefficient (W/m^2 °C)
r_a	aerodynamic resistance to mass transfer (m/s)
T_{leaf}	leaf temperature (°C)
T_{air}	air temperature (°C)
k	thermal conductivity (W/m °C)
F	view factor
J	radiosity

temperature and the total heat flux through the roof by means of evapotranspiration [2,10,11,16]. Evapotranspiration is a combined process of water loss from the soil (evaporation) and plants (transpiration). Previous research studies have quantified evapotranspiration with weighing lysimeters that directly measure water loss by using a load sensor or scale [17–21]. Alternatively, a few studies have used soil water balance approach [22,23]. The soil water balance is performed by tracking changes in the substrate water content that can be measured with probes based on different measurement methods [17]. In summer conditions, previous studies have calculated that the green roof evapotranspiration absorbed approximately 12–25% of the incoming heat flux, for a dry and wet green roof, respectively [16]. Another study observed evapotranspiration heat fluxes as high as 350 W/m^2 of roof surface area during the peak solar radiation [20,21]. These results show the importance of evapotranspiration in the reduction of thermal loads on a green roof.

There have been previous experimental efforts to understand heat transfer involving plants [24–27] and develop analytical models to predict transpiration over perforated plates [25]. The plates simulate plant resistance to evaporation [25] or the convective studies helped understand the effect plants have on natural and/or forced convection in greenhouses [26,27]. Nevertheless, even with the recently rehabilitated interest in green roofs in North America, our literature review found only two laboratory experiments, which have evaluated green roof thermal performance in two wind tunnels [13,28]. The first wind tunnel study investigated the evaporative cooling effect of green roof samples [28], while the second study calculated R-values for green roof samples [13]. None of these studies were able to measure evapotranspiration rates continuously.

Overall, previous field and laboratory studies have proved that green roofs can significantly decrease the heat flux through a roof. Furthermore, evapotranspiration is found to play a major role in controlling heat gains through the green roof. However, to the best of our knowledge, there is not one single study that has measured all of the important heat and mass transfer processes simultaneously. Such a comprehensive experimental study represents a challenging task required to enable development and validation of green roof heat transfer model components, as well as the existing evaluations of the overall model performance. This paper presents a new experimental apparatus designed and constructed to collect experimental data in an environmental chamber that houses the apparatus. The experimental data were used to validate a predictive heat and mass transfer model for green roofs [29].

2. Heat and mass transfer fluxes

The energy balance for a green roof can be generalized as following [30,31]:

$$R_n = \dot{Q}_{ET} + \dot{Q}_{sensible} + \dot{Q}_{conduction} + S_{thermal} + M \quad (1)$$

In Eq. (1), the net radiative flux (R_n) represents the total incoming/outgoing solar and long-wave radiation. The evapotranspiration (Q_{ET}), a latent heat flux by convection, represents soil evaporation and plant transpiration water loss. The sensible heat flux by convection ($Q_{sensible}$) is the heat flux between a roof and the surrounding air. The conductive heat flux through a roof ($Q_{conduction}$) represents the heat transfer though a roof. Moreover, the thermal storage capacity of plants is typically neglected by most green roof and soil-vegetation models, which is small when compared to the thermal storage capacity of the soil layer. In this study, the thermal storage ($S_{thermal}$) is neglected by assuming quasi steady-state heat transfer, which is correct for slowly changing environmental conditions similar to the experimental conditions in our environmental. In addition, the metabolic storage (M) is neglected because it typically represents around 1–2% of the net radiation [30,32,33].

Previous studies in urban [34], suburban [35], and agricultural environments [36] have measured ratios of latent, sensible, and conductive fluxes divided by the net incoming radiation. These measured ratios showed the importance of evaporation in Eq. (1) to decrease conductive heat fluxes through the substrate. Table 1 summarizes the results from these different outdoor experimental studies [34–36], and compares them to data collected in a laboratory environment [32]. As shown in Table 1, even in dry suburban conditions, the ratio of evapotranspiration to the net radiation is still significant. The results for ET/R_n ratios for the suburban (wet) and agricultural areas are lower than the results found in controlled laboratory experiments with plants, having ET/R_n equal to 0.86 [32]. Table 1 also shows that each heat transfer mechanism may have an important role in the heat flux reduction depending on the water content in the substrate.

3. Experimental setup

Based on the presented literature review, a new experimental apparatus was needed to address shortcomings in the existing data sets available to create a complete energy balance for green roofs. The new apparatus, named "Cold Plate", was designed and built to include laboratory-rated instrumentation and to allow simultaneous measurements of all important heat and mass transfer processes on a green roof.

The design and construction of experimental apparatus for testing green roof thermal properties was a challenging process that included several versions of the apparatus [37]. The design of the new apparatus was inspired by "Hot Plate" C177 and "Hot Box" C1363 ASTM standards [38,39]. The final version of the "Cold Plate" apparatus uses an environmental chamber and its advanced controls system to monitor and supply different environmental conditions. This is achieved by supplying air at a constant flow rate with a variable supply air temperature and humidity to control

Table 1
Heat flux ratios of sensible heat, soil conduction, and latent heat divided by the net radiation in suburban and agricultural areas compared to heat flux ratios in a laboratory experiment.

	Suburban area (dry) [35]	Suburban area (wet) [35]	Urban area [34]	Agricultural area [36]	Laboratory environment [32]
$Q_{sensible}/R_n$	0.69	0.27	0.36	0.21	0.14
$Q_{conduction}/R_n$	0.07	0.03	0.60	0.05	N/A
Q_{ET}/R_n	0.25	0.70	0.04	0.72	0.86

environmental parameters, such as supply and/or return air temperature and humidity. These tasks were performed by the chamber dedicated Heating, Ventilation, Air-Conditioning (HVAC), and humidification systems [12]. In addition to the HVAC system, a bank of lamps installed inside the chamber serves as a radiative heat source to simulate outdoor short-wave radiation. Consequently, the environmental chamber eliminates most of the non-steady state problems encountered in the field experimentation. This setup also allows the use of laboratory-rated acquisition equipment, which is particularly important for accurate measurements of evapotranspiration because the noise of instrumentation available for field data collection is close to the measured water loss rates. A schematic representation of the "Cold Plate" apparatus inside the environmental chamber is shown in Figs. 1a and 1b, which are not drawn to scale. As shown in Figs. 1a and 1b, thermistors were located at 4 different planes with 5 thermistors placed at each plane, resulting in a total of 20 thermistors. For each measurement plane, one thermistor was placed at the center, and the other 4 thermistors were placed at the center of each quadrant as shown in Fig. 1b. The thermistors at each plane were aligned to be approximately at the same vertical line (Fig. 1a). The further details and instrumentation specifications are provided in Section 3.1.

Additionally, as shown in Fig. 1a, solar radiation is simulated with a bank of very high output (VHO) fluorescent lamps. The box, supporting the green roof sample, is well insulated underneath and uses Styrofoam rigid insulation ($R \approx 8.9$–10.7 m^2 K/W or 50–60 ft^2 h °F/Btu) on its sides to maintain a one-dimensional heat flux. Below the green roof sample, the Cold Plate consists of a copper plate attached to a serpentine heat exchanger that was built by a series of copper pipes specifically assembled for this experiment by Trox Technik. This system was maintained at relatively constant and quasi-uniform temperature with a hydronic system supplying cold water at a constant flow rate of 200 ml/min and temperature of 16–17 °C by a dedicated laboratory PolyScience portable chiller independent of the environmental chamber controls and located outside of the environmental chamber. This temperature was limited by the dew point temperature to avoid condensation, which would introduce noise into the measurements of the green roof sample weight changes. The temperature difference between the opposite sides of the copper plate was approximately between 1 °C and 1.5 °C. However, the actual temperature at the bottom of the substrate changed from experiment to experiment. The temperature at the bottom of the substrate was between 20 °C and 26 °C depending on the heat flux removed by the Cold Plate.

This setup represents summer conditions when the indoor building air is typically cooler than the outdoor environmental air. Underneath the box, a platform is continuously measuring the weight of the green roof sample to quantify the water loss rates.

3.1. Variables measured and instrumentation

The "Cold Plate" apparatus is instrumented with laboratory rated data acquisition sensors. Fig. 1a shows locations of several data acquisition sensors installed in tested green roof samples. The measured parameters of interest are [40]:

1. Evapotranspiration rates – This study measured evapotranspiration by two different approaches:
   (a) Changes in weight of the green roof sample due to the water losses measured with a high-resolution Sartorious IS 300 IGG-H platform with an uncertainty of ±0.010 kg. Evapotranspiration was calculated using the following equation:
   $$\dot{Q}_{ET} = \frac{Weight_2 - Weight_1}{time_2 - time_1}\frac{i_{fg}}{Area} \quad (2)$$
   where $Weight_2$ and $Weight_1$ are in kg and represent the weight difference between $time_2$ and $time_1$ (in s). The time difference used in this study was 2 h. i_{fg} is the enthalpy of vaporization (J/kg) and Area is the green roof sample area (m^2).
   (b) Changes in substrate volumetric water content (VWC) due to the water losses measured with a Campbell Scientific CS616-L water content reflectometer. The water content of the substrate was calculated using an in-house calibration specifically developed for the substrate analyzed in this study. Evapotranspiration was calculated using the following equation:
   $$\dot{Q}_{ET} = \frac{VWC_2 - VWC_1}{time_2 - time_1}\frac{\rho_{water} \times Vol_{substrate} \times i_{fg}}{Area} \quad (3)$$
   where VWC_2 and VWC_1 are the non-dimensional volumetric water content of the substrate and they provide an average water content difference between $time_2$ and $time_1$ (in s). Time difference in this study was 2 h. $Vol_{substrate}$ is the volume occupied by the substrate (m^3), and ρ_{water} is the water density (kg/m^3).
   A third approach to measure evapotranspiration was tested in a previous version of the "Cold Plate" by measuring the supply and exhaust air humidity. However, this approach did not work due to the chamber size and air humidifier controls, and as a result the noise in collected data was the same order of magnitude as the measured evapotranspiration rates [37]. The reliable evapotranspiration data used in this study came from the data measured by the scale.
2. Incident incoming short-wave radiative fluxes – Measured by a Kipp&Zonen CPM11 secondary class (best accuracy possible, ISO 9060 classification) pyranometer with spectral range of 285–2800 nm and expected daily uncertainty of less than 2%.
3. Incident incoming long-wave radiation – Measured by a laboratory-rated Kipp&Zonen CGR4 pyrgeometer with spectral range of 4500–42000 nm. The long wave measurements are confirmed by simplifying the complex radiative heat exchanges between multiple surfaces in the chamber. The proposed simplified model is based on a radiative heat analyses among three surfaces: (1) lamps, (2) plants and (3) chamber walls surrounding green roof sample as explained in Section 3.3.1.
4. Outgoing long-wave radiative fluxes– Calculated using measured average surface temperatures of the plants and substrate, as well as using plant emissivity of 0.97 [41] and substrate emissivity of 0.95 [42].
5. Heat fluxes through the green roofs – Measured by heat flux meters and by making an energy balance for the "Cold Plate". The Thermonetics Corporation H 01-18-3-E heat flux

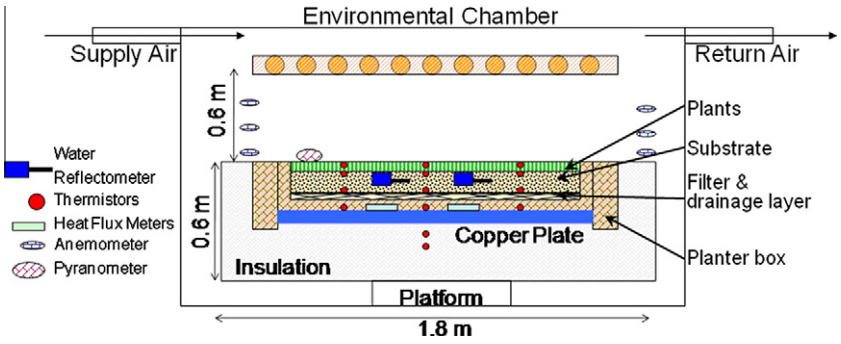

Fig. 1a. "Cold Plate" apparatus inside the environmental chamber: vertical cross section.

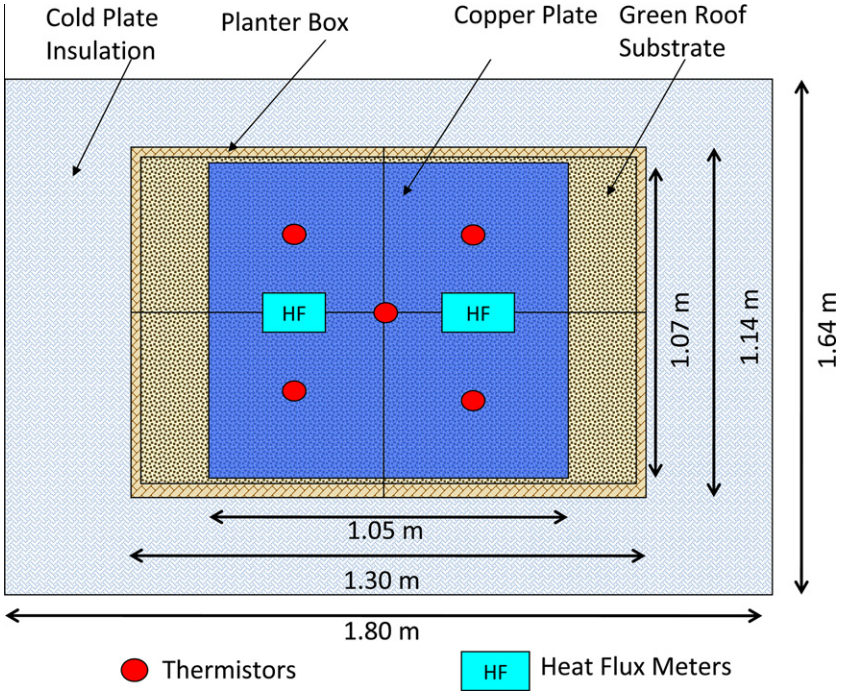

Fig. 1b. "Cold Plate" apparatus inside the environmental chamber: horizontal cross section.

meters had a calibrated uncertainty of 3% and 0.11× 0.11× 0.004 m^3 dimensions. In addition to discrete measurements of heat fluxes through the green roof sample based on two heat flux meters, the heat flux was also measured as an integral value for the sample via the overall energy balance for the heat exchanger sitting underneath the sample. The measured energy balance had an overall uncertainty of 10–15% depending on the accuracy of the measured water temperatures and water flow rates for the Cold Plate heat exchanger. The method consists of measuring the incoming and outgoing "Cold Plate" water temperatures using Omega 910-44034 thermistors with ±0.1 °C uncertainty, and water flow rates using McMillan Model S-113 micro-turbine with ±5% uncertainty.

6. Convective heat transfer fluxes – Calculated by subtracting all measured heat flows in the total energy balance equation (1).
7. Substrate top and bottom layer temperatures – Measured with thermistors. The surface top layer temperature was measured by a set of 5 Omega 44033 thermistors with an uncertainty of ±0.2 °C. These thermistors were protected with a plastic cover because they were located under a thin layer of substrate to measure the top substrate temperature. The surface bottom layer temperature was measured with 5 HOBO TMC20-HD thermistors with an uncertainty of ±0.25 °C using a HOBO U12 series of data logger. These thermistors were located at the bottom of the substrate layer in contact with the filter cloth membrane.
8. Substrate thermal conductivity – Calculated from the measured heat flux through the substrate and the measured temperatures at the top and bottom layers of the substrate.
9. Plant temperatures – Measured by 4 Omega 44033 thermistors (uncertainty of ±0.2 °C) attached to plant leaves. An infrared camera was used during the last day of experiments to confirm the surface temperature values.
10. Average VWC – Measured by Campbell Scientific CS616-L water content reflectometers. They were diagonally inserted in the green roof substrate to measure the average volumetric water content of the green roof substrate.
11. Air velocities – Measured with omnidirectional hot-sphere anemometers at different locations around the green roof samples. The Sensor Electronic omnidirectional probes

(HT-412-0) with transducers (HT-428-0) have a velocity uncertainty of ±0.02 m/s. The same sensors measured air temperature close to the "Cold Plate".

12. Room air relative humidity levels and temperatures – Measured with humidity and temperature sensors located in the chamber supply and return ductwork. The relative humidity sensors were the Vaisala HUMICAP® Humidity and Temperature Transmitter Series HMT330 with an uncertainty of ±1.0% RH for a measuring range of 0–90% RH. The supply and return temperatures were measured with Omega thermistors 44033, having an uncertainty of ±0.2 °C. Humidity ratio was calculated from the return air measurements and assumed to be uniform in the entire environmental chamber, which is a reasonable assumption as chamber had mixing ventilation system.
13. Spectral reflectivity of green roof samples – This measurement was done outside of the "Cold Plate" apparatus as it required more space. The measured reflectivity for the samples with plants includes combined plant and substrate reflectivity. Thus, the measured reflectivity values are representative values for the reflectivity of a green roof sample, rather than the reflectivity of a particular component (substrate or plants). The reflectivity was measured with an ASD Inc. FieldSpec® 3 Portable Spectroradiometer at 90° angle (calibrated lamp directly above plants). The reflectivity for the visible (400–700 nm), near infrared (700–1200 nm), and most of the solar spectrum (350–2300 nm) are respectively 0.03, 0.27 and 0.06. More details about these results are available in the literature [40]. For the samples without plants, the variable substrate reflectivity for the specific wavelength of the lamps was obtained from the literature for different soils and plants [32,43,44]. Future research will measure the spectral reflectivity of different samples with different substrates and plants.
14. Leaf area index (LAI) – Measured manually by leaf count and measuring leaves dimensions in several grid points for sample with *Delosperma nubigenum*. LAI for the sample with *Sedum spurium* was obtained using: (1) the Food and Agriculture Organization of the United Nations (FAO) equation depending on plant height [45] and (2) correlation between Normalized Difference Vegetation Index (NDVI) and LAI for several ecosystems such as tundra and desert. NDVI is a ratio of spectral surface reflectance for red and near-infrared radiation, which gives an estimate of vegetation cover or LAI [30].

From this list of 14 measured variables, evapotranspiration and conductive heat fluxes were measured by two independent approaches enabling the assessment of accuracy for both measurement methods. This focus is due to the fact that evapotranspiration has a major role in the heat and mass transfer phenomena at green roofs, while the conductive fluxes quantify reduced energy demand for space conditioning. Overall, the "Cold Plate" apparatus represents a new experimental setup that simultaneously measures all of the important heat fluxes on a green roof sample for quasi-steady state heat and mass transfer analyses.

3.2. Green roof samples

The tested green roof samples consist of planter boxes that are 1.3 m wide and 1.14 m long. The substrate depth was approximately 0.09 m. A relatively large width and depth compared to the sample thickness were selected to assure a one-dimensional heat flux through the sample. In addition, only the core part of the green roof sample was used for thermal measurements, as shown in Fig. 1b. The surrounding part of the sample was used as a buffer zone where one-dimensional flux is less likely. Finally, the green roof samples were originally planted and grown in a greenhouse, while the fully grown samples were moved into the environmental chamber for testing.

The length and width of the tested samples are not representative of a real green roof size, and certainly there are similarities issues when comparing a sample to real green roofs. Therefore, we used materials typically used in the green roof industry, and followed the main idea of available ASTM testing methods designed to assess material performance under main driving forcing, while keeping in mind that the real installations have their one influencing factors on material performance. Furthermore, the "Cold Plate" experimental setup mimics typical conditions of a green roof surrounded by air rather than surrounded by another solid surface. In addition, the heat and mass transfer processes are the same for a real green roof and tested samples. The intension of this study was to quantify these transfer processes for future validations and adjustments in real green roof installations.

The substrate used in the green roof planter boxes consisted mainly of expanded clay, a typically used substrate in green roofs. The selected substrate saturates at VWC of approximately 0.55 and has the field water content capacity of approximately 0.34 [6]. The density of the substrate was calculated to be 640 kg/m^3, which is similar to other reported green roof substrate densities [6,20,46]. Plants selected for our experiments were *D. nubigenum* and *S. spurium*. These drought tolerant species were selected as they are typical plants used on extensive green roofs. These two species are hardy, succulent plants and have the ability to survive in drought conditions by limiting their water loss due to transpiration [3]. Below the substrate, the samples had Enkadrain filter and drainage layer to filter and drain all excess water from the green roof samples. Finally, the samples contain a water proof membrane to protect the planter boxes from the water damage. LAI measured at the end of the experiments was 2.7, with an average height of 5 cm. This measurement was done only at the end as it is an intrusive, destructive, and time-consuming approach because the measurements are done manually by leaf count and size measurement in several areal sections for the sample with *D. nubigenum.*

3.3. Environmental conditions and experimental procedure

Three different green roof samples were tested: (1) green roof sample without plants, (2) green roof sample with *S. spurium*, and (3) green roof sample with *D. nubigenum*. The sample without plants was tested to compare heat fluxes between the samples without plants and the samples with plants while detailed results of this comparison are presented in two previous publications [11,12]. Furthermore, two different types of lamps were used: (1) 165 W UVA tanning lamps and (2) 160 W VHO Daylight Fluorescent lamps. The UVA lamps were initially selected because they provided a higher irradiance. However, the amount of UVA radiation was significantly higher than what is naturally available in the outdoor environment. In fact, the sample plants started to wilt after a single 3-day test. Therefore, the remaining experiments with sample plants used Daylight Fluorescent lamps. These types of lamps have an almost constant wavelength output in the visible range compared to the Cool White or Warm White that have a higher output in the yellow–orange–red part of the spectrum [47].

Each experimental test started by watering the samples until saturation was reached at 48 and 24 h before starting the experiments. Lamps were programmed to turn on/off at the same time each day. All tests had 14 h of artificial lighting and 10 h of darkness, except for the UVA experiments, during which there was an equal time of artificial lighting and darkness. These "day/night" cycles created cooler temperatures during the dark periods to simulate outdoor conditions. Data from the last 2 h of "daylight" were used to calculate steady-state values for all of the heat transfer processes.

Quasi-steady state conditions were obtained at the end of the daylight period for most measured variables. The selection of the 14 h for artificial lighting was a combination of a time length necessary to obtain quasi-steady state conditions and day–night conditions present in nature. Different variables reached quasi-steady state conditions at different times. Evapotranspiration achieved quasi-steady state faster and the heat flux through the green roof was the last one. Thus, this study used the last 2 h of measured data because the variables that achieved steady state earlier remained almost constant. In this way, quasi-steady conditions were reached for all variables of interest, except for substrate water content. It is important to mention that this is a dynamic system that is always changing as the water content changes due to evaporation.

A total of eight experiments were successfully conducted using the samples with plants. Table 2 shows environmental conditions for performed experiments with plants and without plants that are discussed in previous publications and are presented in Table 2 only for the purposes of comparison [11,12,40]. All environmental conditions outlined in Table 2 were obtained by the environmental chamber controls system. Table 2 does not include supply air conditions, as the HVAC and humidification systems were continuously changing these values to keep the return temperature and relative humidity at the setpoints. It is important to notice that the environmental conditions in the chamber are the same as return conditions due to the presence of the mixing ventilation system. For each experiment, one of the following environmental variables was changed at a time: (1) relative humidity, (2) solar radiation, (3) wind speed, (4) air speed, (5) air temperature and (6) plant type. These changes were introduced to quantify their effects on heat fluxes due to each individual environmental variable and to enable evaluation of green roof thermal performance for different environmental conditions.

Table 2 shows a Baseline I case scenario, which represents the benchmark case. The Baseline experiment was replicated twice for control purposes (Baseline I and Baseline II). The Baseline scenario targeted dry bulb temperature and relative humidity equal to 28 °C and 30%. This condition is similar to the Annual Cooling Design conditions for San Francisco, California [48]. As shown in Table 2, most of the actual environmental conditions were very close to the designed or targeted conditions. However, solar irradiance at plant height slightly changed from experiment to experiment. Furthermore, there was a difference between air temperature measured near the plant layer and the chamber return air temperature. This temperature difference is due to the air stratification close to the green roof sample because the lamps were a major heat source inside the chamber.

3.3.1. Incoming short-wave and long-wave radiation

The average short-wave incoming radiative flux was measured at the beginning and at the end of the experiments in 36 locations of sample surface at the plant level. The average short-wave irradiance at the core area was 160 W/m^2 when the UVA lamps were operating. In addition, the irradiance measured in the core area deviated less than 10% from the peak value. The average irradiance at the core area when the Fluorescent Daylight lamps were operating decreased from 120 W/m^2 to 70 W/m^2 over the span of several months. This decrease in incoming radiation is due to the decline in the lamps' natural output with time. The total time span between the first experiment with the fluorescent lamps (without plants) and the last experiment (Baseline II) was about seven months. In addition, during all green roof tests, the pyranometer was installed at one side of the green roof samples. The core area average irradiance fluxes were calculated using recorded values from the square area and using a linear relationship between both initial and final contour map studies [40]. Table 2 shows these irradiance values in the fifth column.

Long-wave radiative fluxes were measured with a pyrgeometer and calculated from surface temperature measurements assuming the three surfaces with homogenous temperature: lamps, surrounding walls and the green roof. The model is defined using Eqs. (4)–(9) as defined in the literature [49]:

$$\dot{Q}_{IR,GR} = -F_{21}(J_{GR} - J_{lamps}) - F_{23}(J_{GR} - J_{lamps}) \tag{4}$$

$$\dot{Q}_{IR,lamps} = -F_{12}(J_{lamps} - J_{GR}) - F_{13}(J_{lamps} - J_{walls}) \tag{5}$$

$$\dot{Q}_{IR,walls} = -F_{32}(J_{walls} - J_{GR}) - F_{31}(J_{walls} - J_{lamps}) \tag{6}$$

$$\dot{Q}_{IR,GR} = \frac{-(E_{b,GR} - J_{GR})}{\varepsilon_{GR}(1-\varepsilon_{GR})} \tag{7}$$

$$\dot{Q}_{IR,lamps} = \frac{-(E_{b,lamps} - J_{lamps})}{\varepsilon_{lamps}(1-\varepsilon_{lamps})} \tag{8}$$

$$\dot{Q}_{IR,walls} = \frac{-(E_{b,walls} - J_{walls})}{\varepsilon_{walls}(1-\varepsilon_{walls})} \tag{9}$$

where $\dot{Q}_{IR,GR}$, $\dot{Q}_{IR,lamps}$ and $\dot{Q}_{IR,walls}$ stand for incoming long-wave radiation to the green roof, lamps, and the walls respectively. J_{GR}, J_{lamps}, and J_{walls}, stand for radiosity of the green roof, lamps, and the walls respectively. Finally, $E_{b,GR}$, $E_{b,lamps}$, and $E_{b,walls}$, stand for long wave radiation emitted by the green roof, lamps, and the walls respectively. ε is the surface emissivity. The view factors (F) were calculated assuming a view factor for a 3-D parallel rectangle between the lamps and the green roof as well as using the reciprocity relationship, and summation rule. The view factors resulted from these calculations are:

F_{12} = 0.3306
F_{13} = 0.6694

Table 2
Summary of environmental conditions for green roof experiments inside of the environmental chamber.

Experiment	Air temp. above green roof sample (°C)	Return air temperature (°C)	Return air relative humidity (%)	Short-wave irradiance (W/m^2)	Air speed (m/s)	Plant species[a]
1. Baseline I	32.3	28.1	31	98	0.12	A
2. Humidity	32.2	28.0	46	92	0.11	A
3. Solar	31.2	27.9	33	56	0.10	A
4. Speed	29.0	28.3	32	84	1.08	A
5. Temperature	29.2	26.1	34	71	0.10	A
6. Temperature	24.5	23.9	46	65	0.60	A
7. Baseline II	31.5	27.7	33	86	0.13	A
8. UVA	35.9	32.0	39	158	0.14	B
9. UVA soil	37.4	32.60	38	189	0.17	C
10. Baseline I, soil	32.2	28.10	36	107	0.12	C

[a] A – *Delosperma nubigenum*; B – *Sedum spurium*; C – No plants.

F_{21} = 0.5050
F_{23} = 0.4950
F_{31} = 0.8157
F_{32} = 0.1843

The average incoming long-wave radiation in the core area was 630 W/m^2. Likewise, the calculated incoming long-wave radiation using lamp and wall temperature is 580 W/m^2. The average value of long-wave radiative fluxes for the experiment with fans is 560 W/m^2, while the calculated value is 540 W/m^2. In both cases, the calculated value based on the simplified 3-surface radiative heat transfer provided good results.

3.3.2. Redundancies in Cold Plate experiments

Evapotranspiration was measured with two different methods: scale weight measurements and soil water balance. The total water losses measured from the substrate water balance method were 10–20% larger than the scale readings. Thus, this study used evapotranspiration rates measured from the scale because (a) the scale method is the only method that directly measures evapotranspiration, (b) the substrate water balance is an indirect and less precise technique, and (c) the substrate water balance method results in negative evapotranspiration rates at the beginning of each experiment, which is physically incorrect. These negative evapotranspiration rates would mean that the substrate is gaining weight by condensation. However, a careful analysis of the dew point temperature inside the chamber revealed that all surface temperatures inside the chamber were higher than the dew point temperature, so condensation was not physically possible. In addition, the scale did not detect any weight gain that would indicate negative evapotranspiration rates.

Heat fluxes through green roof substrate were recorded by two different techniques: (1) heat flux meters, and (2) heat balance for the "Cold Plate". Each technique has its tradeoffs. On the one hand, the heat flux meter performance depends heavily on good surface contact. Additionally, heat flux meters have a disadvantage of possibly disturbing the temperature field and adding an error into the measurements [50]. On the other hand, the heat balance method could potentially carry more uncertainties due to additional lateral heat losses on the "Cold Plate". Furthermore, the overall heat balance depends on the accuracy of readings from three sensors: (1) supply water thermistor, (2) return water thermistor, and (3) water flow meter, all installed in the copper plate heat exchanger of the "Cold Plate" apparatus. The potential uncertainties of the heat balance method were minimized by heavily insulating the experimental box ($R \approx 8.9$–10.7 m^2 °C/W or 50–60 ft^2 h °F/Btu) and using accurate water thermistors (uncertainty of ±0.1 °C or ±0.2 °F).

Overall, the heat fluxes calculated with the heat balance across the "Cold Plate" were about 15% larger than the heat fluxes measured by the heat flux meters. In this study, data from the heat balance method was selected for the analyses using the last 2 h of the 14 h daylight cycle to ensure quasi-steady state was accomplished. This method was selected because one of the two heat flux meters installed in the "Cold Plate" apparatus provided unrealistic readings while the heat balance method calculation provided always reliable results and represents the total heat flux through the roof.

4. Experimental data analyses

After analyzing and comparing all different experimental techniques, the next task was the analysis of heat and mass transfer processes in the tested green roof sample. The analyzed fluxes are evapotranspiration, conduction, net radiation, and convection. In addition, substrate and plant surface temperatures are examined due to their role in the overall heat transfer through a green roof assembly. Finally, the time constant for the green roof system is also calculated.

4.1. Evapotranspiration

Evapotranspiration occurs when there is a vapor pressure differential (VPD) between the plants and surrounding air. Due to the VPD presence, water vapor is transferred from the plant leaf surface or substrate into the air by diffusion and convection. This transport phenomenon can be represented by a resistance to vapor transfer in the surrounding air, r_a, present in the denominator of Eq. (10). Most of the water losses in plants are through plant stomata that are represented by stomatal resistance, r_s. Stomata are adjustable pores on the plant surface that open and close to control water losses, absorb/release CO_2 and release O_2. Plants absorb CO_2 as a component required for photosynthesis. Thus, evaporation and photosynthesis are related, although certain plants such as the *Sedums* have unique characteristics that allow them to open their stomata at night when the water losses are smaller [29,40].

$$\dot{Q}_{ET} = \frac{\rho C_p}{\gamma(r_s + r_a)}(VPD) \tag{10}$$

where C_p is the specific heat at constant pressure of air and $\gamma = C_p P / 0.622 i_{fg}$ is the Psychometric constant that depends on atmospheric pressure and latent heat of vaporization, i_{fg}.

As discussed, the evapotranspiration rates were measured by two independent methods. However, only the scale method using a platform is reported due to its greater reliability. Fig. 2 shows evapotranspiration rates for experiments described in Table 2 and summarized below. Experiments 1–7 were conducted using the green roof sample with *D. nubigenum*. Experiment 8 was conducted using the green roof sample with *S. spurium*:

1. Baseline I: Environmental conditions equal to San Francisco design conditions. Test lasted 4 days.
2. Humidity: Relative humidity increased up to 50% by increasing supply air humidity. Test lasted 4 days.
3. Solar: Solar radiation decreased 50% by turning off approximately 50% of the available lamps. Test lasted 4 days.
4. Speed: Wind speed increased to 1 m/s by setting up the fans inside the environmental chamber. Test lasted 6 days.
5. Temperature: Air temperature changed to 26 °C by decreasing supply air temperature. Test lasted 2 days.
6. Temperature: Air temperature changed to 24 °C by decreasing supply air temperature. Test lasted 2 days.
7. Baseline II: Environmental conditions equal to San Francisco design conditions. Test lasted 6 days.
8. UVA: Solar radiation simulated with UVA lamps. Test lasted 3 days.

Most of the data in Fig. 2 follow a similar trend except for experiment number 8. The difference is likely because this experiment used UVA lamps with higher UVA/visible ratio and different plant species, *S. spurium*. In fact, the sample plants started to wilt after only a single 3-day test. Moreover, comparing the behavior of the *Sedums* in experiment 8 with a similar experiments without plants a conclusion can be drawn that plant evapotranspiration was suppressed [12,40]. In contrast, experiments number 1–7 follow a very similar trend that can be divided in 3 stages:

1. Evapotranspiration rates are high and almost constant up to VWC of approximately 0.14.
2. Evapotranspiration decays linearly with volumetric water content up to approximately 0.07.

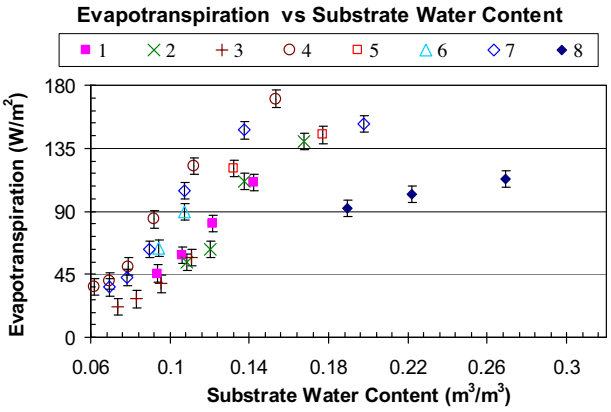

Fig. 2. Evapotranspiration rates for the sample with *Delosperma nubigenum* (experiments 1–7) and *Sedum spurium* (experiment 8) (the error bars represents uncertainty measurements from the scale).

3. Evapotranspiration rates decrease slower than evapotranspiration rates in the previous stage, and this slow decrease is nonlinear when VWC is lower than 0.07.

The evapotranspiration rates could be measured based on the weight and/or substrate water content measurement. A linear relationship could be expected for evapotranspiration and the substrate water content as it is the case for evaporation and the substrate water content. However, the measured curves in Fig. 2 show that plants have a nonlinear behavior due to different variables affecting their water loss, such as photosynthesis and associated stomatal resistance. In principle, the curves have an elongated "S" shape with extremely low evapotranspiration rates when the water is scarce and really high evapotranspiration rates when the water is abundant in the substrate (Fig. 2). In the middle of the substrate water content range, the relationship is approximately linear.

These three evapotranspiration stages can also be observed during day and night variations, as shown in Fig. 3 (a) and (b). Fig. 3(a) shows 10-min averaged evapotranspiration rates for Baseline II experiment. Fig. 3(b) presents 10-min averaged evapotranspiration rates and VWC for the Baseline II experiment vs. time. In Fig. 3(b), both evapotranspiration rates and VWC decreased with time, because of the drying of the substrate due to water evaporation. The gray areas denotes the 10-h dark periods during experiments. Fig. 3(a) and (b) was created from the weight measurement as explained in Section 3.1. As shown in Fig. 3(a), the green roof sample achieved the largest and nearly constant evapotranspiration rates during the first two days, or when VWC was above 0.14. Fig. 3(a) and (b) shows that there is also evapotranspiration during the night periods. However, day/night evapotranspiration ratio is about 3 when substrate is wet and about 5 when substrate is dry. Larger evapotranspiration during the day periods could be attributed to the short-wave radiation warming the leaf surfaces that promoted a higher vapor pressure deficit with the surrounding environment. This also affects the stomatal resistance, which depends on solar radiation, temperature, humidity and water availability [40,31]. Additionally, there is also some substrate evaporation, but it is typically lower when the samples are completely covered by plants [12,40]. Finally, data in Fig. 3(a) at low substrate water content seems to have "shorter" day or night periods. This visual issue stems from the inferior resolution of the water content sensors compared to the resolution of the scale.

Fig. 2 also shows that evapotranspiration rates obtained from experiments number 1–3 are very similar. However, experiments number 4–7 resulted in larger evapotranspiration rates. The first

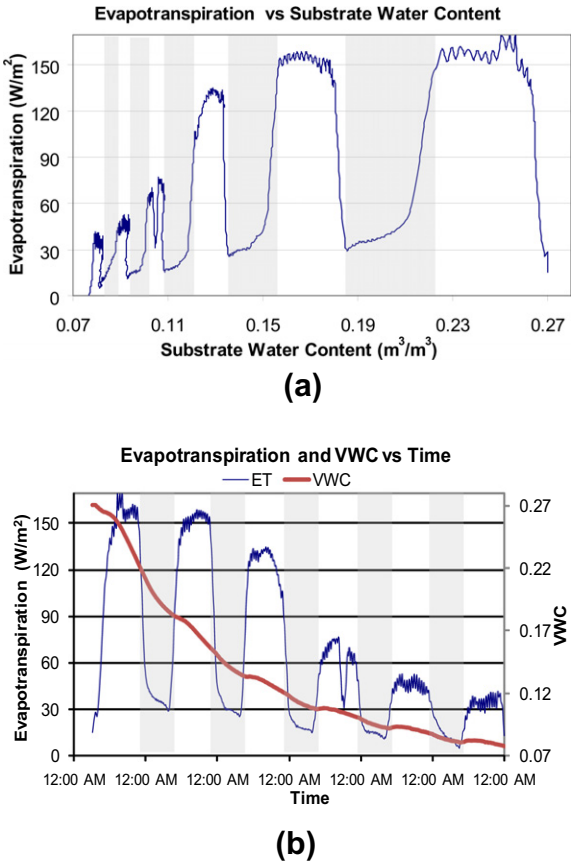

Fig. 3. Ten-min averaged evapotranspiration rates for the Baseline II test versus (a) substrate water content and (b) time (gray areas denote 10-h dark periods during the experiments).

three experiments were conducted in February and early March, while experiments 4–7 were conducted in April. This time between experiments 1–3 and 4–7 allowed plants to grow and increase their LAI. This proves that plant coverage and LAI have a very important role in evapotranspiration.

Among all experiments, experiment number 6 achieved the largest evapotranspiration rates because the air speed was about 9 times larger than the air speed in other experiments. Thus, larger air speeds improved convective mass transfer between the plants and the surrounding air. An increase in the air speed from 0.1 m/s to 1 m/s resulted in an increased evapotranspiration by 10–30%. In contrast, an increase in humidity in the environmental chamber decreased the evapotranspiration fluxes as the vapor pressure difference between the plants and the surrounding air decreased. This is because evapotranspiration is directly proportionally to the vapor pressure differential and inversely proportional to the mass transfer resistances (r_s and r_a) as shown in Eq. (10) [29]. Further analysis of the data has also shown that the relationship between evapotranspiration and vapor pressure deficit is not as strong and apparent as with the substrate water content in Fig. 2 [29,40].

From all of the tested environmental conditions, air speed was the most influential environmental variable. Humidity, solar radiation, and air temperature did not show strong influences on evapotranspiration. However, future experiments with windy and humid conditions could help to prove whether humidity also has an important role.

In conclusion, from all analyzed variables, the substrate water content was the most important factor in determining the evapotranspiration rates. However, radiation is also a very important

factor that was not fully tested due to lamp radiation limitations [40]. Radiation (mainly solar) is the driving mechanism that causes plant evapotranspiration. In fact, both plants' photosynthesis process and plant stomata are sensitive to incoming radiation intensity. Thus, both variables are very important for the overall heat and mass transfer. It is also important to note that Figs. 2 and 3 present measured evapotranspiration, which is the combined plant transpiration and substrate evaporation. Overall, the plant transpiration or latent heat flux depends on the physiological properties of the plants and their stomatal resistance that controls water losses.

4.2. Conductive heat fluxes

Conductive heat fluxes followed the Fourier equation defining that the conductive fluxes are proportional to the thermal conductivity k of the material layer and the temperature difference across the layer as defined in the following equation:

$$\dot{Q}_{conduction} = \frac{k(\Delta T)}{L} \tag{11}$$

where L is the thickness of the green roof substrate.

Previous research has shown that the thermal conductivity of green roof substrates increases as the water content in the substrate increases [11,46]. However, heat fluxes through the substrate shown in Fig. 4 increase as the substrate gets drier. Lower heat fluxes are due to the lower temperature differences that allow for lower heat fluxes, and also allows for higher evapotranspiration fluxes. The latter leads to temperature decrease due to the latent heat used during evaporation, which leads to a lower temperature difference across the substrate. Thus, it appears that the higher evapotranspiration rates overcome the changes in the thermal conductivity. As a result, evapotranspiration plays an important role in redirecting heat fluxes from the roof assembly to the surrounding environment. Based on Figs. 2 and 4, higher short-wave irradiation could lead to higher absorbed radiation, and, consequently, to higher substrate temperatures and higher heat fluxes through the roof. However, a higher short-wave radiation would also result in higher evapotranspiration rates that would consequently decrease the temperature of the plants and the conductive heat fluxes. However, plant transpiration will stabilize after certain irradiation level and will no longer increase with further increase in the short-wave radiation intensity. The threshold for this stabilization depends on the plant type. Unfortunately, such a high irradiation level was not achieved in the presented experiments.

A variable albedo or reflectivity may also play a role, as higher albedo values indicate that a smaller amount of incident radiation is being absorbed by the green roof. The substrate has a lower reflectivity at higher substrate water contents, and a higher reflectivity at lower water contents. Thus, a lower reflectivity at higher water contents can contribute to the higher net radiation. However, as later discussed in Section 4.3, the influence of the variable reflectivity is not as strong as the evapotranspiration rates. This is an important statement since it points to tradeoffs between having a wet or dry green roof to further reduce heat fluxes through a roof assembly.

Additionally, lower conductive heat fluxes were obtained in the experiment with the higher wind speed (experiment number 4). Furthermore, higher conductive heat fluxes were obtained in the Baseline II experiment (number 7) compared to the Baseline I experiment (number 1) despite similar environmental conditions. The increased fluxes are due to the higher net radiation despite the higher evapotranspiration rates in the Baseline II experiment and higher LAI observed and measured after experiment number 7. This is also consistent with the increase in the substrate surface temperatures presented in the next section along with the calculated substrate thermal conductivity.

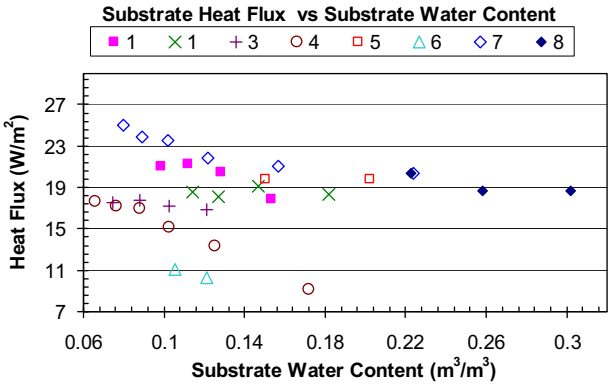

Fig. 4. Measured substrate conductive heat fluxes through the green roof samples.

4.2.1. Substrate and plant surface temperatures

Substrate surface temperatures in Fig. 5 show a similar trend to heat fluxes in Fig. 4. The lowest temperatures were observed when the substrate was wettest. Furthermore, Fig. 6 shows average plant surface temperatures from the 4 thermistors attached to the leaves. The plant surface temperature is consistently higher than the substrate temperature, because plants are providing shading to the substrate. Plant surface temperature is higher when the substrate is drier, for which evapotranspiration redirects a minimal amount of incoming fluxes. Plant surface temperatures are also used to calculate the green roof net radiation. Among all of the experiments, experiment number 6 and 4 resulted in the lowest surface temperatures due to the lower air temperature (experiment 6) and improved convection by the air speed increase (experiment 4). In contrast, experiment 8 obtained the highest temperature because of the higher radiation levels and evapotranspiration was suppressed due to UVA radiation.

It is important to mention that plant surface temperatures shown in Fig. 6 were obtained with thermistors attached to the leaves. Unfortunately, this technique might not measure plant temperature very accurately, despite the thermistors' uncertainty of ±0.2 °C. This is because only half of the sensor area is in contact with the leaf and the other half is exposed to air temperature and incoming radiation. Incoming radiation was minimized by coating the thermistors with aluminum foil. However, to address this weakness in the temperature measurement, an infrared (IR) camera was used during the last day of experiments to take infrared pictures of the green roof samples. Point to point comparison between the thermistors and IR camera readings showed that the readings from the IR camera were consistently higher by 1–2 °C, but within the measurement uncertainty of the IR camera of ±2 °C. The same difference was observed when comparing average plants' surface temperature obtained from the thermistors and the average temperature obtained from the camera. Moreover, standard deviation of the plants' surface temperature from small sample sections was around 0.7–1 °C, compared to standard deviation of 1.4–2 °C for the entire green roof area sample.

Fig. 7 shows the measured plant, substrate surface temperatures and the calculated wet bulb temperature (WBT) using the return air temperature and return air relative humidity for the green roof samples with and without plants. The graph is divided into 9 parts because it is arranged per experimental test. The vertical axis shows the average daily quasi-steady state measured or calculated temperature and the horizontal axis shows the experiment number, which assigns a number to each day that the green roof sample

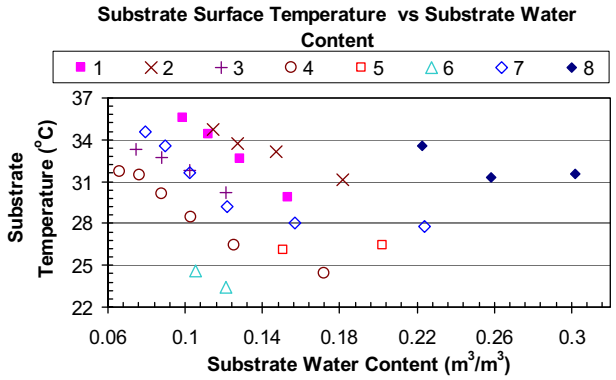

Fig. 5. Substrate top temperatures for the green roof sample.

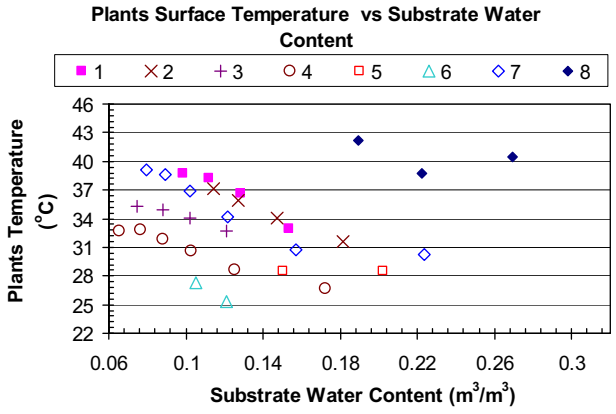

Fig. 6. Plant surface temperatures for the green roof sample.

was test, following a chronological order. For example, "Soil UVA" has 6 square points that represent the measured values for the experiments without plants and using UVA lamps. "Soil UVA" also has the first six experiment numbers, which refer to 6 days that the experiment was taking place on.

As shown in Fig. 7, the measured plant and substrate temperatures were higher than the calculated wet bulb temperatures. However, the data show a tendency to approach the web bulb temperature during the first day of experiments, when the green roof samples were the wettest. Thus, plant and substrate temperature could asymptotically approach the wet bulb temperature when the plant surface and substrate top layer are wet.

4.2.2. Substrate thermal conductivity

The substrate thermal conductivity of the green roof samples with and without plants was calculated using (1) the heat flux measurements through the substrate and (2) the measured temperature difference across the green roof substrate. The substrate thermal conductivity for the green roof samples without plants was obtained from a previous study before testing the samples with plants under similar environmental conditions to Baseline I (experiment 1) and UVA (experiment 8) as shown in Table 2 [11,12]. Fig. 8(a) shows the calculated substrate thermal conductivity for all experiments and Fig. 8(b) shows the calculated substrate thermal conductivity for all the experiments with temperature difference across the substrate higher than 7 °C. The dark, continuous line in Fig. 8(a) represents the linear regression fitted from about 3/4 of the calculated thermal conductivities, excluding experiments 5–7. Once the data points with low temperature difference across the substrate are deleted most of the data follow a linear equation, which is very similar to the one calculated by another field study using a green roof substrate with similar densities [14]. Overall, the conductivity values are lower than previously reported for different substrates/soils [51,52], which is reasonable because green roof substrates based on expanded clay have higher porosity and larger fraction of air pockets than other typical soils.

4.3. Net radiation

Net radiation depends on the spectral properties of the green roof, such as reflectivity, but also on the incoming short-wave radiation, temperature of the plants, sky (in this case lamps and surrounding walls) as well as substrate. Moreover, depending on environmental conditions, net radiation can be positive for the incoming fluxes or negative for the outgoing fluxes, when there is no short-wave radiation. Fig. 9 shows the net radiation for the samples with plants. The experiments with UVA lamps resulted in the higher net radiation values possibly because of the higher efficiency and slightly higher lamp power output (165 W) compared to the daylight fluorescent power output (160 W). UVA lamps also contained a special coating that directs most of the radiation downwards, in contrast to the more diffuse radiation of daylight fluorescent lamps. It is also important to mention that measurements of the incoming long-wave radiation were not performed with the UVA lighting system. Thus, the values shown here are based on the assumption that the total output (long and short

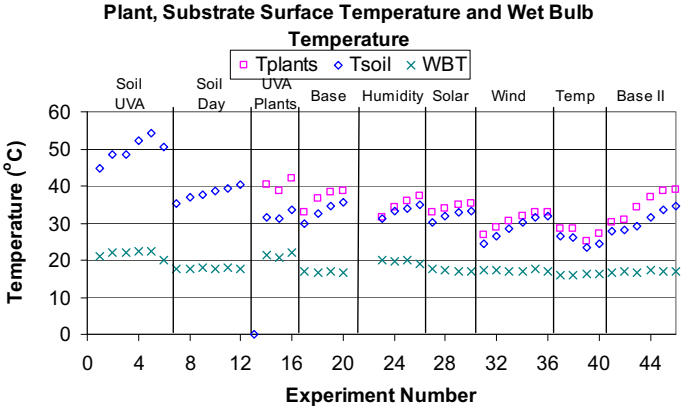

Fig. 7. Plant (squares), substrate (circles) surface temperatures and calculated wet bulb temperature (WBT, crosses) for the green roof sample without and with plants.

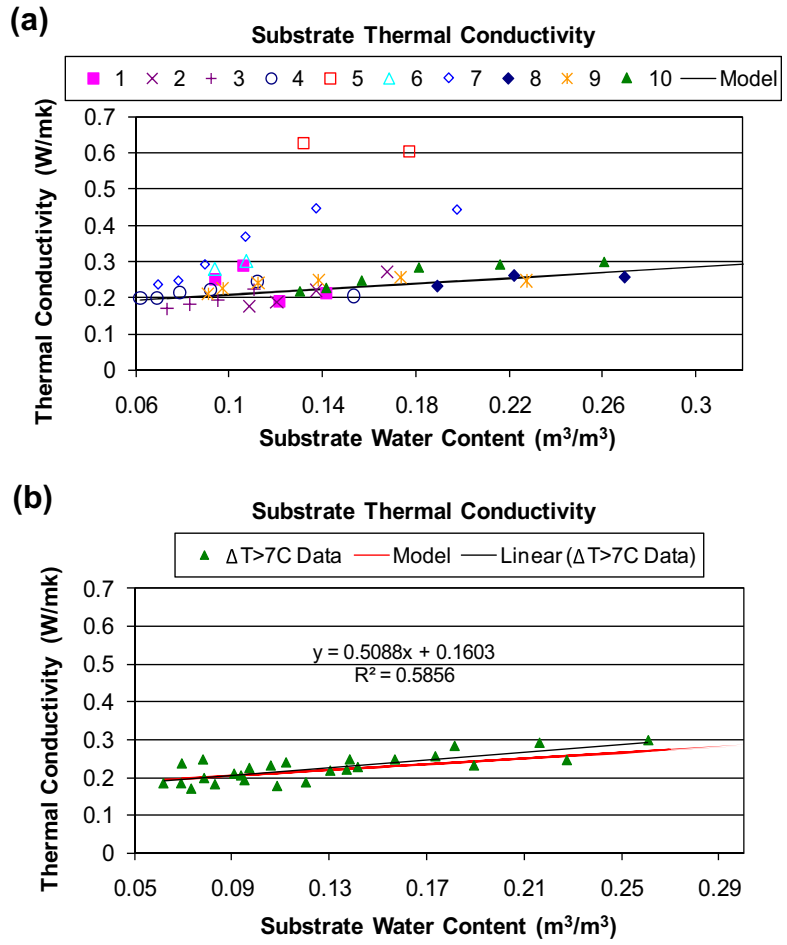

Fig. 8. Calculated substrate thermal conductivity for (a) the green roof sample with plants (1–8) and without plants (9, Soil UVA; 10 Soil Day) and (b) samples with a substrate temperature difference greater than 7 °C.

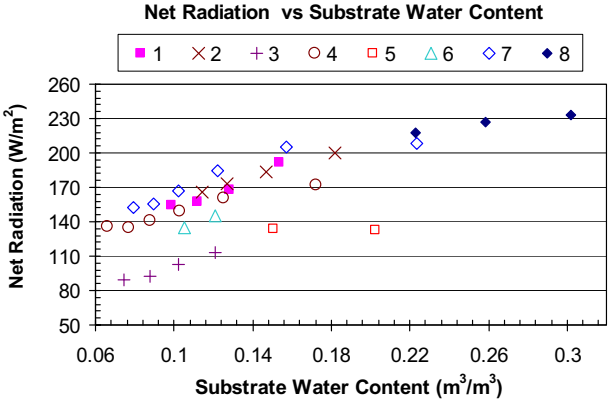

Fig. 9. Net radiation for green roof samples with plants.

wave radiation) of the UVA and fluorescent lamps should be similar with just a minor correction due to the different input power (165 W/160 W).

Overall, most plant experiments have a very similar net radiation, except the experiments with about 50% of lamps being turned off (experiment 3). The largest net radiation was recorded for the wet sample conditions, when plant temperature is the lowest, as shown in Fig. 9, and the reflectivity is the lowest [40]. The net radiation decreases as the substrate water content decreases. This is mainly due to the increase in plants and substrate temperatures. The highest net radiation was observed with higher water contents because this lead to higher evapotranspiration rates, which resulted in lower substrate/plant temperatures. This in turn reduced the outgoing long-wave radiation leaving the green roof sample, thus increasing the overall incoming long-wave radiation. From all experiments, the largest net radiation observed was during the Baseline II experiments (experiment 7), which were slightly higher than the net radiation in Baseline I (experiment 1). This explains the higher conductive heat flux through the green roof observed in Fig. 5. The higher net radiation is related to the higher surface area of the plants due LAI increase with time as plants were growing during the course of experiments. Once the net radiation is known and all other heat fluxes are known, convection is calculated by making an energy balance for the green roof samples using Eq. (1) and Fig. 10.

4.4. Convective heat fluxes

Fig. 11 shows convective heat transfer for the samples with plants. Convective heat fluxes are calculated indirectly by subtracting all of other measured fluxes from the total measured heat flux. Thus, convection is the least accurate heat flux measured by the "Cold Plate", having a calculated uncertainty of ±11 W/m^2 [53]. Convective fluxes are typically calculated using Eq. (12), although in this study, they were calculated using Eq. (1). In Eq. (12), the convective heat flux is proportional to the temperature difference between surface (T_{plants}) and surround air (T_{air}) and the convective

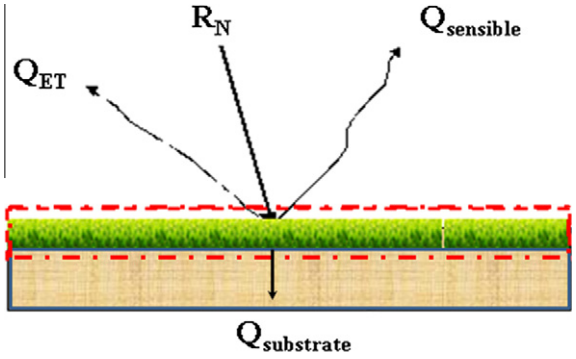

Fig. 10. Boundaries across energy balance applied to green roof samples with plants.

heat transfer coefficient, h_{conv}. Furthermore the convective heat transfer coefficient depends on several factors such as air speed and temperature difference. The conductive heat flux is calculated as following:

$$\dot{Q}_{sensible} = h_{conv}(T_{plants} - T_{air}) \quad (12)$$

In the present study, the experiments with the highest air speed (test 4) have the smallest values of the convective heat transfer rate. This interesting and unexpected outcome is due to the relationship between evapotranspiration and convection. The increase in air speed improved not only transport of heat, but also of water vapor. This phenomenon caused higher evapotranspiration fluxes, which reduced the available heat gain from the net radiation to the rest of heat fluxes, such as convection and conduction. In other words, due to the fact that the incoming short-wave radiation flux was kept almost constant in the experiments, the increase in evapotranspiration affected the other heat fluxes in the heat balance (Eq. (1)), which in turn decreased the convection heat flux. Moreover, the higher evapotranspiration rates decreased the plants temperature, which consequently decreased convection fluxes. Thus, the increase in the air speed increased the convective heat transfer, but at the same time, it decreased the temperature difference between the plants and the surrounding air.

For all cases, convection follows an opposite trend from the evapotranspiration trend. Thus, larger convection fluxes were observed at drier substrate conditions, when the evapotranspiration fluxes are minimal. Similar results were also found with higher wind speeds [53].

4.5. Time constant for the tested green roof sample

"Day/night" cycles provide adequate conditions to calculate the time constant of the green roof samples because the temperature inside the chamber remains almost constant at 28 °C during "daylight" hours. Thus, the time constant for the green roof samples was also calculated based on the amount of time required for heat fluxes through the green roof sample to achieve steady-state conditions. The time constant (τ) is a measure of how a system responds to environmental changes. In this study, the time constant was defined as: (1) time required for the initial heat flux to increase 2/3 of the difference between the heat flux at the beginning of the day and the quasi-steady state value, and (2) $\tau = \rho \cdot Volume \cdot C_p/h \cdot Area$, as defined in the literature [49]. The calculated time constant using definition (1) varied from 3.9 h to 6 h having an average of 4.9 h. The calculated time constant using definition (2) was about 4.3 h. However, the time constant could be as low as 1–2 h at actual roof conditions when the wind speeds and convective heat transfer coefficients are much higher.

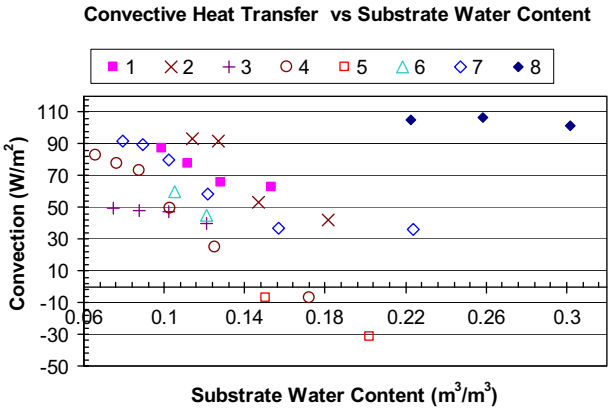

Fig. 11. Convective heat transfer for the sample with plants.

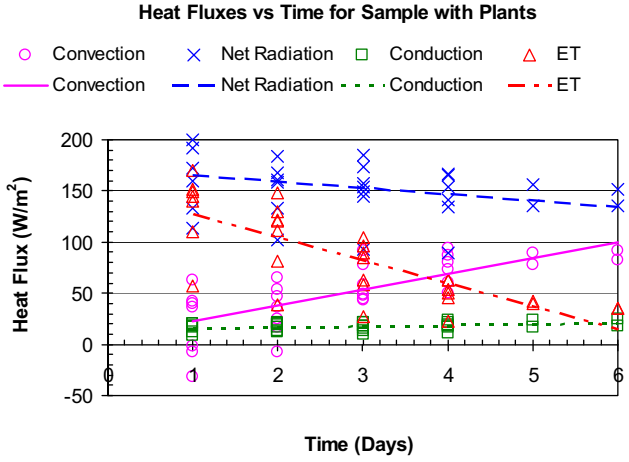

Fig. 12. Measured heat fluxes for the green roof sample with plants represented with individual data points and trend lines (time axis represents the days after the experiments started).

4.6. Discussion of experimental results

All analyzed heat fluxes are compiled together in Fig. 12 for the experiments with plants. In Fig. 12, quasi-steady fluxes are plotted versus the time length starting at the beginning of each experiment. All heat fluxes are interconnected and dependent on each other. Among all heat fluxes, the net radiation is the main incoming flux, or driving flux. Evapotranspiration has a role of controlling the intensity of all others fluxes, by modulating or diverting incoming/outgoing heat fluxes depending on the plant and environmental conditions. It is also interesting to observe how convection follows the opposite trend from the evapotranspiration trend. This opposite trend is caused by increased convection fluxes as plant surface temperature increases. This increase in plant temperature also increases the long-wave radiation emitted from the plants, thus also reducing the net radiation. Likewise, the plant surface temperature increases as evapotranspiration decreases, due to the decrease in the plants ability to convert sensible to latent heat fluxes as the substrate dries. Finally, compared to convection or evapotranspiration, conductive heat fluxes are the least susceptible to water content. This is due to the added resistance to heat transfer by the substrate and plants. Therefore, most of the incoming heat flux gets diverted out of the green roof. However, the lowest conductive heat fluxes through the green roof were consistently found when the green roof was the wettest. The presented exper-

Table 3
Measured energy flux ratios of sensible heat, substrate conduction, and latent heat divided by the net radiation in "Cold Plate" green roof experiments.

	Green roof sample without plants (wet)	Green roof sample without plants (dry)	Green roof sample with plants (wet)	Green roof sample with plants (dry)
$Q_{sensible}/R_n$	0.29	0.40	0.23	0.57
Q_{soil}/R_n	0.21	0.32	0.09	0.14
ET/R_n	0.50	0.28	0.68	0.29

iments prove that lower heat fluxes through the roof samples are obtained when the green roof is wet.

Fig. 12 graphically represents the energy balance defined in Eq. (1). Fig. 12 also shows dynamic and complex heat and mass transport interactions between plants and the environment. This graph is unique because it presents all of the individual heat fluxes continuously measured during several days of complex heat and mass transfer processes. These measurements revealed tradeoffs between convection and evapotranspiration, driven by incoming radiation, modulated by the substrate water content, and resulting in different conductive fluxes through green roof samples.

Table 3 summarizes all of the measured heat fluxes for both green roof samples without plants and with plants. The samples with plants show an average heat flux reduction of 25% compared to samples without plants. In addition, the lowest conductive heat flux occurred at the wettest conditions, with an average reduction of 16% compared to fluxes occurring during dry conditions. Moreover, the measured changes in heat flux ratios shown in Table 3 for the dry to wet sample with plants are very close to the measured ratios for dry and wet suburban areas shown in Table 1. This is an encouraging finding because it shows that the experiments in the environmental chamber were able to represent close to actual outdoor conditions with the "Cold Plate" apparatus.

The reader should be careful in trying to extrapolate these results for design of real green roofs because this study analyzed green roof samples without insulation and under lower short-wave radiation fluxes in order to obtain material properties and model equations in controlled and repeatable environmental conditions. A real green roof on a roof top would be subjected to higher surface temperatures and rapid changes in radiative fluxes. Moreover, code requirements for insulation on the roof would decrease the thermal impact plants would have on green roofs. Additionally, the thermal mass added by the green roof would shift and decrease peak roof temperatures, and minimize potential night cooling of the roof when air temperatures and long-wave radiation cool down a white or a dark roof. Finally, if the vegetation is well established on a real green roof, it capabilities to reduce the incoming radiative fluxes would not diminish with time in the same way that the reflectivity on white roofs decreases due to soiling. All of these realistic roof considerations will play a role in a real green roof and could be done with a validated green roof model.

At the practical level, these results can be applied to the design of a green roof. For example, the data presented here have been used to validate a green roof model [29,40] and could be used as a benchmark for other green roof models. Moreover, the results presented here strengthen the argument of having well-established plants and not only substrate to protect the roof. The results could also help taking further steps to keep the green roof irrigated, to obtain the maximum benefits from the green roof. Because the evapotranspiration has been proven to be the most important factor that reduces heat transfer through the roof, a designer could design a green roof using plants that have low stomatal resistance or higher evapotranspiration rates, if irrigation and water resources are available.

5. Conclusions

A new apparatus was designed and built to simultaneously and continuously measure heat and mass transfer processes for green roof samples inside an environmental chamber. Overall, more than 10 experiments were conducted with a "Cold Plate" apparatus inside an environmental chamber. The experimental data revealed that evapotranspiration has a dynamic and complex behavior that strongly depends on leaf density per roof area or leaf area index (LAI), short-wave radiation and substrate water content. In particular, our study found that evapotranspiration controlled the intensity of all other heat fluxes by modulating incoming/outgoing heat fluxes, depending on the plant and environmental conditions. This finding justified the use of such a complex experimental setup that was able to measure evaporative fluxes with sufficient accuracy to quantify its role in other heat and mass transfer mechanisms.

Experimental data revealed an interesting relationship between water and energy because the samples with higher water content provided higher latent (evapotranspiration) heat fluxes and lower sensible (convective) heat fluxes. This water and energy flux relationship also affected the conductive heat flux through the green roof because the lowest conductive heat fluxes were consistently found when the green roof was the wettest. The conductive fluxes for wet samples were around 16% lower than those fluxes for dry samples. This finding addressed the old dilemma regarding the heat flux tradeoffs between a dry and a wet green roof assembly. Furthermore, our experiments showed that the surface plant and substrate temperature could not be modeled as wet bulb temperature in steady state conditions. The wet bulb assumption could perhaps be true when there is no solar radiation heating up the plants or after a heavy rain event, when the plants and substrate are completely saturated with water. Finally, in the current laboratory setup, the samples with plants consistently show an average heat flux reduction of 25% compared to samples without plants because plants provide extra shading to the roof, additional water storage, and better water control mechanisms based on evapotranspiration and photosynthesis process that occurred in plants.

Acknowledgements

We would like to thank Dr. Robert Berghage, Director of the Penn State Center for Green Roof Research, for his cooperation and assistance with the design and selection of green roof plants and substrate. This study was supported by the Center for Environmental Innovation in Roofing, Washington DC, USA, CONACYT (Consejo Nacional de Ciencia y Tecnologia), Mexico, ASHRAE Graduate Student Grant-In-Aid and ASHRAE Technical Committee TC 4.4 Building Materials and Building Envelope Performance, the National Science Foundation (NSF Grant No. CMMI-0900486) and in-kind donation of TROX Technik, Vaisala Inc, and Kipp&Zonen.

References

[1] S.W. Peck, C. Callaghan, Greenbacks from green roofs: forging a new industry in Canada, Prepared for: Canada Mortgage and Housing Corporation, Environmental Adaptation Research Group, Environment Canada, 1999.

[2] K.K.Y. Liu, B.A. Baskaran, Green roof infrastructure – technology demonstration, Monitoring and Market Expansion Project, Institute for Research in Construction, 2004, B1054.1.
[3] E.C. Snodgrass, L.L. Snodgrass, Green Roof Plants: A Resource and Planting Guide, Timber Press, Portland, 2006.
[4] B. Bass, B.A. Baskaran, Evaluating rooftop and vertical gardens as an adaptation strategy for urban areas, Institute for Research in Construction, NRCC-46737, Toronto, 2003.
[5] K.K.Y. Liu, B.A. Baskaran, Thermal performance of green roofs through field evaluation, in: Proceedings for the First North American Green Roof Infrastructure Conference, Awards and Trade Show, Chicago, 2003, pp. 1–10 (NRCC-46412).
[6] J. Denardo, Green roof mitigation of stormwater and energy usage, M.S. Thesis, The Pennsylvania State University, State College, PA, 2003.
[7] N.H. Wong, H. Cheong, H. Yan, J. Soh, C.L. Ong, A. Sia, The effects of rooftop garden on energy consumption of a commercial building in Singapore, Energy Buildings 35 (4) (2003) 353–364.
[8] K.K.Y. Liu, J. Minor, Performance evaluation of and extensive green roof, in: Proceedings for the Third Annual International Greening Rooftops for Sustainable Communities, Conference, Awards & Trade Show, Washington, DC, 2005, CD.
[9] J. Sonne, Evaluating green roof energy performance, ASHRAE J. 48 (2006) 59–61.
[10] N.H. Wong, P.Y. Tan, Y. Chen, Study of thermal performance of extensive rooftop greenery systems in the tropical climate, Building Environ. 42 (2007) 25–54.
[11] P.C. Tabares-Velasco, J. Srebric, The role of plants in the reduction of heat flux through green roofs: laboratory experiments, ASHRAE Trans. 115 (2) (2009) 793–802.
[12] P.C. Tabares-Velasco, J. Srebric, Heat fluxes and water management of a green and brown roof: laboratory experiments, in: Proceedings for the Seventh Annual International Greening Rooftops for Sustainable Communities Conference, Atlanta, GA, 2009.
[13] H. Bell, G. Spolek, Measured energy performance of green roofs. in: Seventh Annual International Greening Rooftops for Sustainable Communities Conference, Atlanta, GA, 2009.
[14] M. Perino, V. Serra, M. Filippi, Monitoraggio del comportamento termico di un tetto verde: primi risultati sperimentali, Congresso nazionale ATI 2003, Padova, Italy, 2003, pp. 1873–1883.
[15] M. Perino, V. Serra, M. Filippi, Monitoraggio del comportamento termico di un tetto verde: procedura di misura e relative problematiche, ATI 2003 Conf., Padova, Italy, 2003, pp. 1863–1872.
[16] R.M. Lazzarin, F. Castelloti, F. Busato, Experimental measurements and numerical modeling of a green roof, Energy Buildings 37 (2005) 1260–1267.
[17] G. Rana, N. Katerji, Measurement and estimation of actual evapotranspiration in the field under Mediterranean climate: a review, Eur. J. Agron. 13 (2000) 125–153.
[18] M. Schmidt, Energy saving strategies through the greening of buildings the example of the Institute of Physics of the Humboldt University in Berlin-Adlershof, RIO 3 – World Climate & Energy Event, Rio de Janeiro, Brazil, 2003.
[19] M. Koehler, Energetic effects of green roofs to the urban climate near to the ground and to the building surfaces, International Green Roof Congress, Stuttgart-Nürtingen, 2004.
[20] F. Rezaei, Evapotranspiration rates from extensive green roof plant species, M.S. Thesis, Agricultural and Biological Engineering, The Pennsylvania State University, State College, PA, 2005.
[21] R. Berghage, A. Jarrett, D. Beattie, K. Kelley, S. Husain, F. Rezai, B. Long, A. Negassi, R. Cameron, W. Hunt, Quantifying evaporation and transpiration water losses from green roofs and green roof media capacity for neutralizing acid rain, National Decentralized Water Resources Capacity Development Project, 2007.
[22] N.D. VanWoert, D.B. Rowe, J.A. Andresen, C.L. Rugh, L. Xiao, Watering regime and green roof substrate design affect Sedum plant growth, HortScience 40 (3) (2005) 659–664.
[23] H. Takebayashi, M. Moriyama, Surface heat budget on green roof and high reflection roof for mitigation of urban heat island, Building Environment 42 (2000) 2971–2979.
[24] P.H. Schuepp, Tansley review No. 59. Leaf boundary layers, New Phytol. 125 (1993) 477–507.
[25] J.N. Cannon, W.B. Krantz, F. Kreith, D. Naot, A study of transpiration from porous flat plates simulating plant leaves, Int. J. Heat Mass Transfer 22 (1979) 469–483.
[26] M. Aubine, J. Deltour, Natural convection above line heat sources in greenhouse canopies, Int. J. Heat Mass Transfer 37 (12) (1994) 1795–1806.
[27] R.T. Atarassi, M.V. Folegatti, R.P. Camponez do Brasil, Convection regime between canopy and air in a greenhouse, Sci. Agricola (Note) 63 (1) (2006) 77–81.
[28] S. Onmura, M. Matsumoto, S. Hokoi, Study on evaporative cooling effect of roof lawn gardens, Energy Buildings 33 (2001) 653–666.
[29] P.C. Tabares-Velasco, J. Srebric, A heat transfer model for assessment of plant based roofing systems in summer conditions, Building Environ. (in press), doi:10.1016/j.buildenv.2011.07.019.
[30] H.G. Jones, Plants and Microclimate, Cambridge University Press, Cambridge, 1992.
[31] D. Hillel, Environmental Soil Physics, Academic Press, San Diego, 1998.
[32] D.M. Gates, Biophysical Ecology, Springer-Verlag, New York, 1980.
[33] M. Saighi, C. Moyne, A new simplified model of heat and mass transfer in the soil-plant atmosphere system, Int. J. Heat Mass Transfer 41 (11) (1998) 1459–1471.
[34] A. Tejeda-Martinez, Sobre mediciones y parametrizaciones del balance energetico y la estabilidad atmosferica en la ciudad de Mexico, Ph.D. Thesis in Geography, Universidad Nacional Autonoma de Mexico, 1996 (In: V.L. Barradas, A. Tejeda-Martinez, E. Jáuregui, Energy balance measurements in a suburban vegetated area in Mexico City, Atmospheric Environment 33 (1999) 4109–4113).
[35] V.L. Barradas, A. Tejeda-Martinez, E. Jáuregui, Energy balance measurements in a suburban vegetated area in Mexico City, Atmos. Environ. 33 (1999) 4109–4113.
[36] D.E. Anderson, S.V. Verma, N.J. Rosenberg, Eddy correlations measurements of CO_2, latent heat and sensible heat fluxes over a crop surface, Boundary Layer Meteorol. 29 (1984) 263–272.
[37] P.C. Tabares-Velasco, J. Srebric, R. Berghage, Thermal performance of a lightweight tray for the green roof media, in: Fifth Annual International Greening Rooftops for Sustainable Communities, Conference, Awards & Trade Show, Minneapolis, MN, 2007.
[38] ASTM, ASTM C 1363-97, Standard Test Method for the Thermal Performance of Building Assemblies by Means of a Hot Box Apparatus, ASTM International, West Conshohocken, PA, 1997. Available from: <www.astm.org>.
[39] ASTM, ASTM C 177-97, Standard Test Method for Steady-State Heat Flux Measurements and Thermal Transmission Properties by Means of the Guarded-Hot-Plate Apparatus, ASTM International, West Conshohocken, PA, 1997. Available from: <www.astm.org>.
[40] P.C. Tabares-Velasco, Predictive heat and mass transfer model of plant-based roofing materials for assessment of energy savings, Ph.D. Thesis, Dept. of Architectural Engineering, The Pennsylvania State University, State College, PA 2009.
[41] J.L. Monteith, M.H. Unsworth, Principles of Environmental Physics, third ed., Academic Press, London, 2008.
[42] R.A. Pielke, Mesoscale Meteorological Modeling, Academic Press, New York, 2002.
[43] W.J. La, K.A. Sudduth, S.O. Chung, H. Kim, Spectral reflectance estimates of surface soil physical and chemical properties, 2008 ASABE Annual International Meeting, Providence, Rhode Island, 2008.
[44] R. Escadafal, Estimating soil spectral properties (Visible and NIR) from color and roughness field data, in: The Twenty-Third International Symposium on Remote Sensing of Environment, Bangkok, Thailand, 1990.
[45] R.G. Allen, L.S. Pereira, D. Raes, M. Smith, Crop evapotranspiration: guidelines for computing crop requirements, Irrigation and Drainage Paper No. 56, Food and Agriculture Organization of the United Nations, Rome, Italy 1998.
[46] D.J. Sailor, D. Hutchinson, L. Bokovoy, Thermal property measurements for eco-roof soils common in the western US, Energy Buildings 40 (2008) 1246–1251.
[47] A. Ryer, The Light Measurement Handbook, InternationalLight, Newburyport, 1997.
[48] ASHRAE, 2005 ASHRAE Handbook Fundamentals, ASHRAE, Atlanta, 2005.
[49] F.P. Incropera, D.P. Dewitt, Fundamentals of Heat and Mass Transfer, John Wiley & Sons, New York, 2002.
[50] R.J. Goldstein, P.H. Chen, H.D. Chiang, Measurement of Temperature and Heat Transfer, in: W.M. Rohsenow, WJ.P. Hartnett, Y.I. Cho (Eds.), Handbook of Heat Transfer, McGraw-Hill, 1998.
[51] O.T. Faouki, Thermal Properties of Soils, Trans Tech Publications, Germany, 1986. pp. 23–26.
[52] N.H. Abu-Hamdeh, A.I. Khdair, R.C. Reeder, A comparison of two methods used to evaluate thermal conductivity for some soils, Int. J. Heat Mass Transfer 44 (2001) 1073–1078.
[53] T. Ayata, P.C. Tabares-Velasco, J. Srebric, An Investigation of Sensible Heat Fluxes at a Green Roof in a Laboratory Setup, Building Environ. 46 (9) (2011) 1851–1861.